



Metamaterial route to direct photoelectric conversion

Yongzheng Wen, Ji Zhou*

State Key Laboratory of New Ceramics and Fine Processing, School of Materials Science and Engineering, Tsinghua University, Beijing 100084, People's Republic of China

Photoelectric conversion is of essential importance for harvesting the solar energy and detecting the photonic and optical signals. Conventional technique for photoelectric conversion is based on the mechanism of photo-generated carriers in semiconductors. As it depends on a series of indirect and sophisticated physical processes, the efficiency and wavelength applicability are severely constrained by the materials' performance and device construction. Here, we propose a novel metamaterial route to convert the optical energy into dc electric energy directly from the carrier drift driven by electric and magnetic field in electromagnetic wave. The metamaterial is composed of magneto-electric coupling metamolecules with two nested meta-atoms. With the excitation of an intense temporally asymmetric Lorentz force in the metamolecule, the free carriers are driven to accumulate at the physical boundary, which generates an apparent static voltage. With the fundamental avoidance of the complex processes in the conventional indirect mechanisms, this innovative paradigm of direct photoelectric conversion supplies a sound strategy for ultrafast photodetection and all-wavelength optoelectronics with high-design freedom.

Introduction

The conversion of the photonic energy into the electricity builds the foundation of the solar-energy harvesting and photodetection [1–3]. The conventional photoelectric conversion, known as photovoltaic effect, typically involves complex quantum mechanism, including the photon absorption, generation, and migration of the charged carriers, and the separation of electron-hole pair with the built-in potential in the semiconductor junction [3]. This indirect and complicated conversion process asks for the elaborately designed semiconductor device and essentially constrains the efficiency to the Shockley-Queisser limit due to the matching of the photon energy and the bandgap of material [4].

Apart from those indirect mechanisms of photoelectric conversion with the sophisticated combination of multiple physical

processes, a more direct approach, rectenna device, which combines the antenna with the rectifying diode, has been proposed to overcome the efficiency limit of conversion [5] and widely used in low-frequency electromagnetic (EM) regime. With the antenna converting the incident EM wave into an ac signal, the diode can rectify it to the usable dc voltage. Over 90% conversion efficiency can be obtained in the radio frequencies. However, it is tremendously difficult to extend the rectenna to the optical regime due to indirect process and the far too slow response of the diode-based rectification [6–8]. A rarely noticed work on direct photoelectric conversion without diode, known as dynamic Hall effect (DHE), was reported by H. Barlow in 1954 [9]. It was proposed to produce dc voltage via the joint action of dynamic electric and magnetic fields of the obliquely incident radiation. This effect is theoretically exhibited by all conducting materials and applicable to whole EM spectra from microwave to visible frequencies with a very fast response [10–13]. However, its fundamental restrictions, including the

* Corresponding author.

E-mail address: Zhou, J. (zhouji@tsinghua.edu.cn).

weak magnetic component in the EM wave and the inevitable necessity of oblique incidence, significantly erodes the efficiency and makes the DHE remain seemingly silent for over half a century [11,14–16].

On the other hand, the advent of metamaterial supplies a groundbreaking route to reconstruct the spatial distribution of electric and magnetic fields in EM wave with elaborately designed artificial resonant structures [17–20]. Miscellaneous extraordinary physical properties have been realized with the extensive studies on controlling the spatial variation of the electric field [21,22], including the harmonics generation and photonic spin Hall effect [23,24]. Recently, based on the localized redistribution of the magnetic field, which was comparably less-investigated before [25,26], a novel magneto-electric coupling mechanism has been established with a metamolecule comprised of two constitutive meta-atoms [27]. The resonant behavior of the outer meta-atom internally produces an intensive magnetic field, and an induced Lorentz force considerably tailors the electric response of the inner meta-atom. Together with the inspiration of the DHE, this artificial magneto-electric coupling mechanism may potentially lead to a new paradigm of photoelectric conversion and dispense with the limitations of the energy band and parasitic effects of the nature material.

In this work, we propose a metamaterial route to directly convert the optical energy into the dc electric energy from the carrier drift by the electric and magnetic field in the optical wave, by the aid of a metamolecule composed of two nested meta-atoms. By exploiting the locally confined and enhanced magnetic field in the outer meta-atom, an intensive nonreversing Lorentz force is excited in the inner meta-atom under a normal incidence of the radiation, rendering an apparent dc voltage. By alternating the geometry of the metamaterial, the converted voltage could be artificially tailored, demonstrating the ultrahigh design freedom of the direct photoelectric conversion.

Results and discussion

Theoretical conception of the direct photoelectric conversion arising from the metamolecule is shown in Fig. 1(a), and the inner meta-atom is coupled with the localized magnetic field provided by the outer meta-atom instead of the incident magnetic field. With the normal incidence of an EM wave, a dramatically enhanced out-of-plane magnetic field \mathbf{B} is internally generated by the circulating surface currents \mathbf{J} in the outer meta-atom [25]. The carriers of the inner meta-atom would be under an intensive magnetic force \mathbf{F}_B orthogonal to the drift motion driven by the localized electric field \mathbf{E} , establishing the foundation of the evident photoelectric conversion. Since the localized magnetic and electric fields are artificially reconstructed by the metamolecule, the oblique incidence is not necessary. This mechanism is fundamentally distinct from the conventional DHE, which directly results from the weak out-of-plane magnetic field component of the obliquely incident EM wave and presents negligible strength.

The fundamental magnetic force was further studied to reveal the physics behind the direct photoelectric conversion. By substituting the drift velocity $\mathbf{v} = \tilde{\mu}_e \mathbf{E}$, the magnetic force could be evolved as $\mathbf{F}_B = q \tilde{\mu}_e \mathbf{E} \times \mathbf{B}$, where q is the electron charge, and $\tilde{\mu}_e$

is the mobility of the inner meta-atom in the Drude model. As the localized fields originate from the incident EM fields, their amplitudes can be expressed as $B = u(x,y,z)B_i$ and $E = v(x,y,z)E_i$, where $u(x,y,z)$ and $v(x,y,z)$ are the enhancement coefficients for the localized magnetic and electric fields at the coordinate (x,y,z) respectively. The dynamic oscillation of the electric and magnetic fields at the same frequency would break the temporal symmetry of the magnetic force, and a static component could then be acquired as

$$\mathbf{F}_{BS} = \frac{q}{2} \tilde{\mu}_e u(x,y,z)v(x,y,z)E_i B_i \mathbf{a}_g \quad (1)$$

where \mathbf{a}_g is the unit vector indicating the direction of magnetic force. In the steady condition, the constant magnetic force is canceled by an electric force from the built-in electric field \mathbf{E}_y , which could then be expressed as

$$\mathbf{E}_y = \frac{1}{2} \tilde{\mu}_e u(x,y,z)v(x,y,z)E_i B_i \mathbf{a}_g \quad (2)$$

By simply integrating the transverse built-in electric field, the relation between the generated voltage V_{dc} and the incident power density of the EM wave P_i can be obtained as

$$V_{dc} = \mu_0 \tilde{\mu}_e u_{int} v_{int} P_i \quad (3)$$

where μ_0 is the vacuum permeability, u_{int} and v_{int} are the integral values of the $u(x,y,z)$ and $v(x,y,z)$ respectively (see Supplementary note I).

As seen from Eqs. (2) and (3), the enhancement coefficients guarantee the generation of the evident dc signal, which is artificially controlled and manipulated by the design of the metamolecule. By simply transforming Eq. (3), the sensitivity of the generated dc voltage versus the incident power density can be extracted as $S_{dc} = V_{dc}/P_i = \mu_0 \tilde{\mu}_e u_{int} v_{int}$, which is solely determined by the metamolecule and can be potentially used to evaluate and compare the performance of the direct photoelectric conversion.

The equations also indicate some key design rules for the metamaterial. In the first place, improving the mobility of the inner meta-atom would strengthen the photoelectric conversion proportionally, because the free electrons would gain higher drift velocity, leading to a more significant magnetic force. Meanwhile, the high conductivity of the material composing the outer meta-atom would benefit the conversion as well, since it increases the current density and provides stronger localized magnetic field. The low loss materials are preferred in both meta-atoms but with different reasons (See Supplementary Fig. S1). For the outer meta-atom, the lower loss would reduce the Joule heat due to the resonant behavior and provide stronger magnetic field. It is especially important in high-frequency regime, where the dissipation of the metal becomes considerable and may significantly erode the efficiency of the direct photoelectric conversion. For the inner meta-atom, the low loss means less collisions and higher mobility, which would apparently benefit the generation of dc voltage. Another factor that might influence is the generation of the excitons when responding to the EM wave with high photon energy, such as the infrared. The photo-injected electron-hole pairs would increase the conductivity of the inner meta-atom, which may shield the local magnetic and electric fields and decrease the output voltage. The photo-

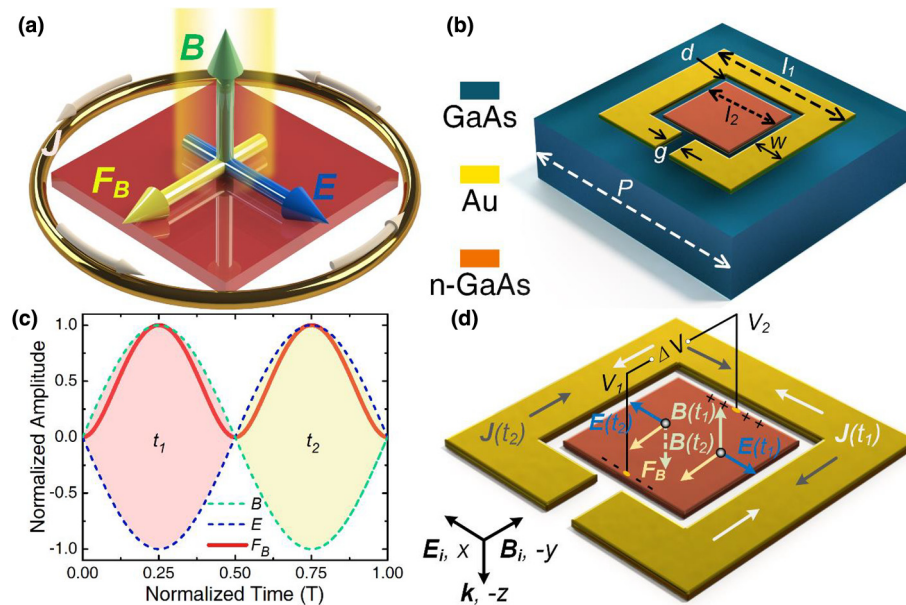


FIGURE 1

(a) The principle of metamaterial-based direct photoelectric conversion: the EM wave is normally incident, and both fields are from the resonance. (b) Schematic of the metamolecule: In terahertz regime, the geometric constants are $P = 30 \mu\text{m}$, $l_1 = 20 \mu\text{m}$, $l_2 = 10 \mu\text{m}$, $w = 4 \mu\text{m}$, $g = 2 \mu\text{m}$, and $d = 1 \mu\text{m}$. (c) The simplified relation among the localized magnetic \mathbf{B} and electric fields \mathbf{E} , and the magnetic force \mathbf{F}_B in time domain. The amplitudes are normalized, and the time is normalized to one period of oscillation T . (d) Dynamic orientations of the circulating currents \mathbf{J} , the localized fields, and the magnetic force with the EM wave illuminating in $-z$ direction. The carriers are assumed as electrons with negative charges. The electric potential difference between the two probes is indicated as $\Delta V = V_2 - V_1$.

induced carriers could be avoided by choosing the material with relatively wide bandgap.

Based on the theoretical scheme, a feasible metamaterial for the direct photoelectric conversion is designed, and the metamolecule is composed of a square meta-atom nested in a splitting (SR) meta-atom, as illustrated in Fig. 1(b). At resonance, a circulating current of the SR meta-atom will induce the enhanced magnetic field, which produces intense magnetic force in the square meta-atom. We assume the carriers in the square meta-atom are free electrons with negative charges, and the simplified relation among the localized magnetic and electric fields, and the magnetic force is plotted in Fig. 1(c). The direction of the local electric field is opposite to that of the incident field due to the resonant behavior of the SR meta-atom, and the dynamic physical process is depicted in Fig. 1(d). At the first half period of oscillation t_1 , the localized magnetic and electric fields, acting on the free electrons of the square meta-atom, result in a magnetic force pointing to the gap of the SR meta-atom. At the second half period t_2 , both fields reverse, and the magnetic force direction remains. Obviously, the temporal symmetry of the magnetic force is broken, and its direction does not reverse with the incident fields. With the unidirectional magnetic force, the free electrons of the square meta-atom accumulate on the physical boundary close to the gap of the SR meta-atom, leaving the equal and positive charges exposed on the other one, which produces a transverse dc voltage across the square meta-atom due to the built-in electric field. It can be found that the realistic process in the metamolecule exactly agrees with the theoretical model.

To verify our theoretical prediction on the photoelectric conversion, an illustrative metamaterial with the same structure

shown in Fig. 1(b) was modeled and simulated with a finite-element method, and its geometrical constants were optimized to work in terahertz (THz) regime. The substrate was modeled as a 10- μm -thick intrinsic GaAs, and the square meta-atom is a layer of 500-nm-thick n-doped GaAs film. The SR meta-atom is comprised of a 500-nm-thick Au film. Two small probes were set in y direction to monitor the dc voltage as indicated in Fig. 1(d). Fig. 2(a) plots the transmission, reflection, and absorption spectra of the metamaterial under normal incidence. The localized magnetic field reaches its maximum at 1.00 THz, which is slightly lower than the resonant frequency of 1.02 THz. The surface currents and magnetic field distributions at 1.00 THz of the metamolecule are shown in Fig. 2(b), corresponding to the first half period (t_1) in Fig. 1(d). The circulating currents produce the enhanced magnetic field as maximum 54 times stronger as the incident one. The induced magnetic field can penetrate through the square due to its thinness, and the surface currents of the square meta-atom are opposite to the incident electric field.

With a continuous plane wave at 1.00 THz normally illuminating from the top, the frequency response of the potential difference between the two ports of the square meta-atom is plotted in Fig. 3(a), and the nonuniformity of the localized magnetic field was taken into account. The amplitude of the incident electric field was set as $1 \times 10^7 \text{ V/m}$, corresponding to the power density of $1.33 \times 10^{11} \text{ W/m}^2$, which can be easily achieved with a current-available table-top THz laser [28–31]. An evident voltage peak of +1.0 mV at 0 Hz could be observed, and this dc signal demonstrates the temporal symmetry of the magnetic force is broken which generates the dc voltage. The positive sign of the

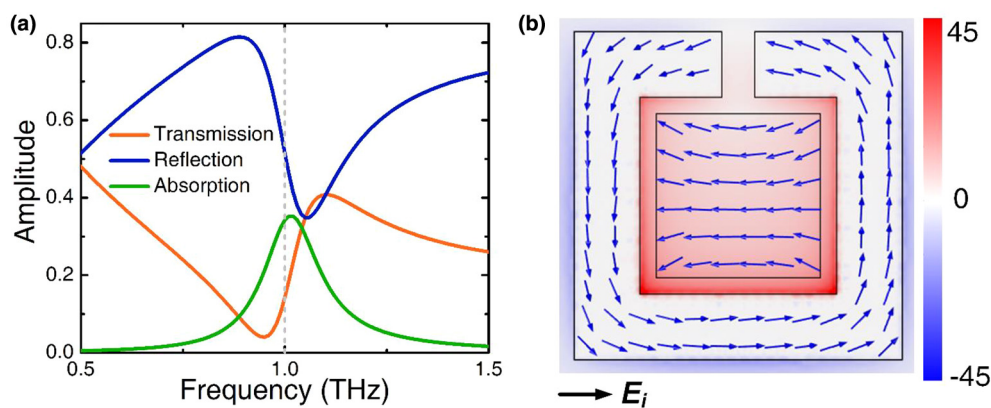


FIGURE 2

(a) The transmission, reflection and absorption spectra of the metamaterial under normal incidence with 1.00 THz marked with gray dashed line; (b) the magnetic field distribution with the scale normalized to the incident magnetic field amplitude. The orientation of the surface currents is marked by the blue arrows with the corresponding direction of the incident electric field indicated.

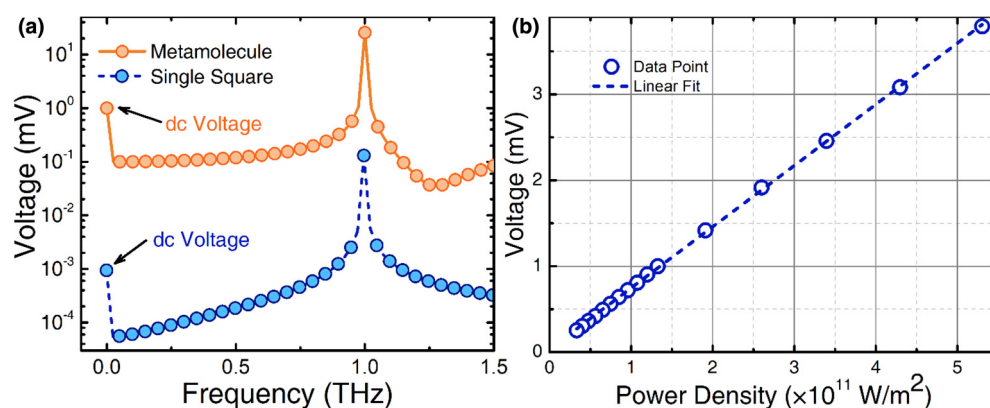


FIGURE 3

(a) The log-scale frequency spectra of the metamolecule under normal incidence of 1.00 THz plane wave and the single square meta-atom under lateral incidence of the same wave; (b) the generated dc voltage of metamolecule as a function of the power density of the incident THz wave.

voltage indicates the nonreversing component of the magnetic force points to the gap, as predicted in the physical model. The other peak at the fundamental frequency of 1.00 THz originates from the harmonic oscillation of free electrons in the square meta-atom. For comparison, a single square meta-atom without the outer split ring was also studied. Under the same normal incidence at 1.00 THz, no static voltage could be obtained due to the lack of the vertical component of the magnetic field (not shown). Under the lateral incidence along the $+y$ direction with the x polarization, the frequency response of the output voltage (Fig. 3(a)) presents two clear peaks including one dc peak of $+0.9 \mu\text{V}$ at 0 Hz as well, arising from the conventional DHE. It manifests that the proposed metamolecule can generate a much more evident voltage, and the strength is enhanced by 1.1×10^3 times.

Fig. 3(b) plots the relation between the output dc voltage of the metamolecule and the power density of the incoming THz wave. A linear fitting can be obtained, which is in fine agreement with the theoretical prediction presented in Eq. (3). The sensitivity of $7.1 \times 10^{-12} \text{ mV}/(\text{W}\cdot\text{m}^{-2})$ can thus be extracted.

To elucidate the fundamental physical mechanism behind the direct photoelectric conversion, the magnetic force distributions for the square meta-atom in the metamolecule were studied. As shown in Fig. 4(a) and (b) respectively, the directions of the local magnetic and electric fields vary at the first and second halves of an oscillating period, but that of the magnetic force in the metamolecule remains, presenting an evident asymmetry in time, which has been fully predicted in theory. For comparison, the magnetic force distribution for the laterally illuminated single square meta-atom was also studied as presented in Fig. 4(c), and its direction is along the incident Poynting vector in $+y$ direction. It can be found that the magnetic force throughout the meta-atom is stronger than the maximum value in the single square. Fig. 4(d) presents the probed temporal responses of the magnetic force density at the same point in the two samples, and the temporal symmetry breaking of the metamolecule with a static component of $32.2 \text{ nN}/\mu\text{m}^3$ could be extracted by the low-pass filtering, which is 215 times stronger than $0.15 \text{ nN}/\mu\text{m}^3$ of the single square. The temporal asymmetry for the metamolecule is almost as perfect as the ideal state in

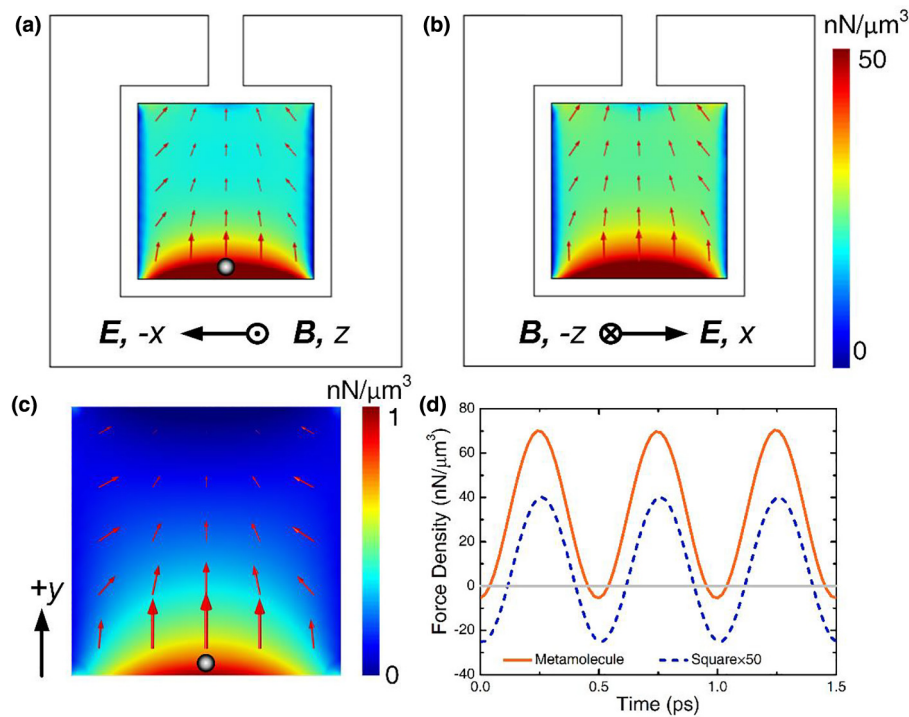


FIGURE 4

The magnetic force density distribution for the square meta-atom in the metamolecule at first (a) and second (b) half period of oscillation, the red arrows indicate the direction of the magnetic force, and the corresponding directions of the local magnetic and electric fields are marked; (c) the magnetic force density distributions for the single square, and the red arrows indicate the direction of the magnetic force, and the direction of the incident Poynting vector is marked; (d) the temporal responses of the magnetic force density at the points marked in (a) and (c), and the $0 \text{ nN}/\mu\text{m}^3$ is marked with gray line.

Fig. 1(c), which is distinctly higher than that of the single square. The intense magnetic force and the explicit symmetry breaking in time guarantee the direct photoelectric conversion in the metamolecule together, which fully supports the proposed theory.

Considering the resonance nature of the metamaterial, we studied the polarization dependence of the generated dc signal as plotted in Fig. 5(a). While varying the incident polarization from x to y , the sign of the voltage remains positive, but its amplitude decreases dramatically because the LC resonance of the SR meta-atom dies out and the localized unidirectional magnetic field vanishes (see Supplementary Fig. S2). This result also implies that the proposed mechanism is distinct from other

helicity-driven photogalvanics such as the circular photogalvanic and the spin-galvanic effects [32,33]. Those effects essentially require the circular polarization, and its chirality would determine the direction of the induced photocurrents. While this direct photoelectric conversion occurs under the linear polarization, and only the amplitude of the output voltage depends on the angle of the polarization, rather than its sign. Additionally, the output voltage is actually from the square meta-atom made of the n-doped GaAs, but the circular photogalvanic effect is forbidden in it due to the spatial inversion symmetry of the material [11].

The influence of the gap size (g) of the SR meta-atom on the converted voltage has also been investigated as shown in Fig. 5

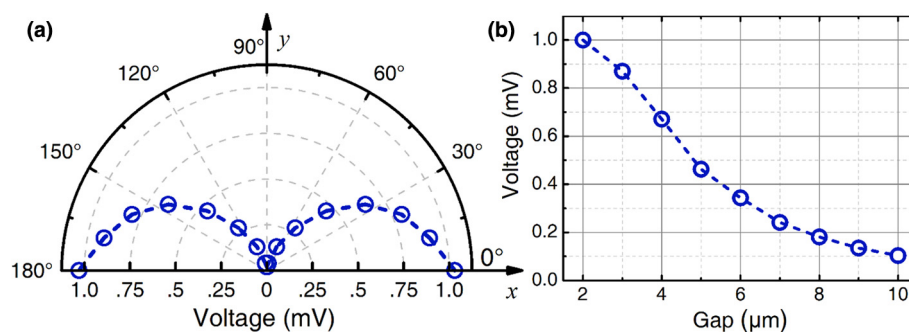


FIGURE 5

(a) The converted voltage as a function of the polarization angle of the incident THz wave with respect to the x axis; (b) the relation of the converted voltage to the gap size of the metamolecule.

(b). By increasing the gap, the resonant frequency of the metamolecule shifts, and the local magnetic field at 1.00 THz decreases due to the dropping strength of the resonance (see [Supplementary Fig. S3](#)), which leads to the monotonic decrease of the generated dc voltage. It can be conveniently predicted that by optimizing the resonance strength of the metamolecule, the photoelectric conversion could be further enhanced, and its properties could be artificially manipulated and designed with ultrahigh freedom by varying the geometry of the metamolecule.

With the realistic materials in the proposed structure, the mechanism of metamaterial-based photoelectric conversion is highly achievable in experiment by microfabrication techniques, and an intense THz laser based on a nonlinear crystal and a femtosecond laser would be a feasible source for the measurement, which can generate THz wave with the peak electric field in the order of 10^9 V/m [29,31]. It should also be noted that the 1 mV output voltage comes from just a single metamolecule. Considering the fact that metamaterial is usually in the form of an array, by connecting all the metamolecules in series, which can be conveniently realized with the currently available techniques (see [Supplementary Fig. S4](#)), the overall output voltage would be orders of magnitude higher than that of the single metamolecule. In our case, a metamaterial with an area of 1 mm^2 could produce an output voltage of 1.1 V ($1\text{ mV} \times 1\text{ mm}^2 / (30 \times 30\ \mu\text{m}^2) \approx 1.1\text{ V}$), which is sufficient to drive an integrated circuit (IC). Since the proposed metamolecule is just a proof-of-concept and not optimal, we believe there is still plenty of room to improve the photoelectric conversion by optimizing the structure. Meanwhile, the compaction and fabrication-friendly compositions of the metamaterial render it suitable for on-chip integration and application.

It should be noted that difference between the proposed mechanism of direct photoelectric conversion and some previously reported integration of metamaterial with other version of Hall effect is intrinsic because the fundamental physics behind the phenomenon is different. For example, a strong photonic spin Hall effect could be achieved by a metasurface, which splits the polarization of light instead of the electron-hole pair in the conventional Hall effect [24]. Dong et al. provided a qualitative prediction on the existence of an all-optical Hall effect based on the dynamic toroidal moment in a cavity-based metamaterial [34], and they considered it as the counterpart of the second harmonic generation [23]. Although they claimed it results from the Lorentz force of the magnetic component of light, the consensus based on the hydrodynamic theory has been reached that the nonlinear response of the metal-based metamaterial is actually dominated by the intrinsic surface contribution of the metal boundary instead of the Lorentz force [35]. In the design proposed here, the direct photoelectric conversion explicitly arises from the temporal asymmetry of the intensive Lorentz force excited by the magneto-electric coupling in the metamaterial structure, instead of the nonlinearity in nature material. In fact, all the compositions of the proposed metamaterial are treated as linear materials in the simulations to avoid the influence of the natural nonlinearity.

As a pure magneto-electric process driven by the Lorentz force, the response of the photoelectric conversion would be ultrafast [36,37]. The response time of the metamaterial is solely

governed by the electron relaxation process of the compositions, ranging from tens of femtoseconds to a few picoseconds in different regimes [38,39]. The response of the metamaterial is thus expected to be in the similar scale (see [Supplementary Fig. S5](#)). The universality of the Lorentz force enables the principle of the direct photoelectric conversion to be applied to all the conducting materials by simply replacing the inner meta-atom with the target material, such as semiconductors, metals, and graphene (see [Supplementary Fig. S6](#)). Consequently, it may become a generic tool for understanding the fundamental electron dynamics in those materials at high frequency, which would substantially advance the research of the semiconductors and two-dimensional materials. The accumulation of the electrons at the physical boundary driven by the temporally asymmetric Lorentz force could also induce some other physical effects. It would locally influence the characteristics of electronic transport due to the increasing density of the electrons, which would affect the conductivity and mobility of the inner meta-atom at the boundary in the macroscopic scale. The accumulated electrons would also produce an apparent static electric field, which may be used to capture and control the motion of the charged particle due to the electrostatic force.

Not limited to the presented metamaterial, the direct photoelectric conversion can be achieved with any artificial structure, if only it satisfies the essential requirements of magnetic field enhancement and magneto-electric coupling as suggested in the physical model (see [Supplementary Figs. S7 and S8](#)). It means that the characteristics of the photoelectric conversion, such as the amplitude and sign of the dc voltage, can be materially optimized, and precisely designed and manipulated with fantastic freedom. Meanwhile, as a pure EM process, the proposed theory can be easily applied to an ultrawide wavelength range from microwave to infrared by simply structuring the inclusion geometry of the metamaterials without the rigid requirement of high enough photon energy (see [Supplementary Fig. S9](#)). These advantages may also inspire myriad possibilities in a variety of other fields, such as ultrafast photodetection, all-wavelength optoelectronics, and ac–dc conversion.

Conclusions

In conclusion, we theoretically demonstrate a novel route to directly convert the optical energy into dc electricity based on metamaterial composed of magneto-electric coupling metamolecules with two nested meta-atoms. An intensive temporally asymmetric Lorentz force is excited by the interaction between the redistributed magnetic and electric fields localized inside the metamaterial, which can produce an evident dc voltage by accumulating the electrons at the physical boundary. An illustrative metamaterial numerically verifies the dc electric energy converted from the normally incident optical wave, and the output voltage is over three orders of magnitude stronger than that of the conventional DHE. This metamaterial-based direct photoelectric conversion, totally avoiding the complex physical processes in the conventional indirect mechanism, may open unlimited application potentialities with the superiorities including high controllability, wide wavelength applicability, fast response, and on-chip integration.

Materials and methods

Materials modeling

The substrate of the metamaterial was modeled as a 10- μm -thick intrinsic GaAs with the lossless permittivity of 12.9. The SR meta-atom is comprised of a 500-nm-thick Au film. The plasma frequency and damping frequency of Au are much higher than the target frequency of 1.00 THz, and its low mobility leads to a negligible impact of the localized magnetic field. Thus, the Au film is simply modeled with the isotropic conductivity of $4.1 \times 10^7 \text{ S/m}$. The square meta-atom is a layer of 500-nm-thick n-doped GaAs film. The free electron carrier density of the n-doped GaAs is modeled as $5 \times 10^{17} \text{ cm}^{-3}$, corresponding to the dc conductivity σ_0 of $3.1 \times 10^4 \text{ S/m}$ and the dc mobility μ_{e0} of $3800 \text{ cm}^2/\text{Vs}$ with the damping frequency γ of $2\pi \times 6.4 \text{ THz}$, and the permittivity at high frequency is 12.9 [40]. To take the localized magnetic field B into account, the n-doped GaAs was modeled with an anisotropic Drude conductivity tensor as [41–43].

$$\tilde{\sigma}(B) = \tilde{\sigma} \begin{pmatrix} \frac{1}{1+\beta^2} & -\frac{\beta}{1+\beta^2} & 0 \\ \frac{\beta}{1+\beta^2} & \frac{1}{1+\beta^2} & 0 \\ 0 & 0 & 1 \end{pmatrix} \quad (4)$$

where $\beta = \frac{\mu_{e0}B}{1-i\omega/\gamma}$, $\tilde{\sigma} = \frac{\sigma_0}{1-i\omega/\gamma}$, and ω is the angular frequency of the incident EM wave. It should be noted that in the anisotropic conductivity tensor, only the z component of the local magnetic field has been considered. This assumption has been made based on the fact that at the resonance, the x and y components of the local magnetic field are much weaker than the predominant z component inside the SR meta-atom, and even weaker than the incident magnetic field, and their influence can be neglected. The anisotropic conductivity tensor has been widely applied in the research related to Hall effect and Lorentz force, ranging from the macroscopic scale to nanoscale [41,42], and its deviation process has been fully described by other researchers[43].

Simulation settings

In both frequency and time domains, single metamolecule was simulated with the periodic boundary condition in x and y directions, and the ports for transmitting and receiving wave were set on the top and bottom boundaries in z direction, respectively. The localized magnetic field was incorporated by inputting the variable representing the local magnetic field when defining the anisotropic conductivity. In this way, the nonuniformity of the localized magnetic field could be fully considered. Two probes were implanted on both sides of the square meta-atom to extract the electric potential difference, as shown in Fig. 2(d).

In the frequency domain, the incident wave was defined as a plane wave in x polarization along $-z$ axis. The S-parameters of the metamaterial were simulated ranging from 0.5 THz to 1.5 THz with the step of 0.01 THz. The reflection (R), transmission (T), and absorption (A) spectra can then be obtained with the relations $R = |S_{11}|^2$, $T = |S_{21}|^2$, and $A = 1 - T - R$.

In the time domain, x -polarized incident plane wave was defined by the electric field $\mathbf{E}_i = (E_{xi}, 0, 0)$, and the expression of E_{xi} is

$$E_{xi} = E(\omega)\cos(\omega t + k_0 z) \quad (5)$$

where $E(\omega)$ is the amplitude of the electric field, t is time, k_0 is the wavenumber at the angular frequency ω , z is the coordinate in z axis. The values used in the time-domain simulations are $E(\omega) = 10^7 \text{ V/m}$, $\omega = 2\pi \times 10^{12} \text{ rad/s}$. The total time of 30 ps was simulated with the step of 20 fs. With the time-domain response, the frequency spectra shown in Fig. 4(a) can be obtained by Fourier transformation.

The single square meta-atom was also simulated in time domain. Under the lateral incidence, the periodic boundary condition was applied in x direction, and the perfect magnetic condition was applied in z direction. The transmitting and receiving ports were set in y direction. The incident wave along $+y$ direction was also defined in x polarization by the electric field, $\mathbf{E}_i = (E_{xi}, 0, 0)$ while the expression of E_{xi} is modified as

$$E_{xi} = E(\omega)\cos(\omega t - k_0 y) \quad (6)$$

The rest parameters are the same as those used in the simulation of the metamaterial, including the amplitude of the electric field and the angular frequency.

Data availability

The raw/processed data required to reproduce these findings cannot be shared at this time as the data also form part of an ongoing study.

Acknowledgments

This work was supported by the Basic Science Center Project of NSFC under grant No. 51788104, as well as National Natural Science Foundation of China under Grant Nos. 51532004 and 11704216, and the China Postdoctoral Science Foundation under Grant Nos. 2015M580096 and 2017T100074.

Declaration of interest

The authors declare no conflict of interests.

Appendix A. Supplementary data

Supplementary data to this article can be found online at <https://doi.org/10.1016/j.mattod.2019.01.001>.

References

- [1] D.E. Carlson, C.R. Wronski, *Appl. Phys. Lett.* 28 (1976) 671–673.
- [2] A. Goetzberger, J. Knobloch, B. Voss, *Crystalline Silicon Solar Cells*, vol. 1, John Wiley & Sons Ltd, 1998.
- [3] L. Enke, Z. Bingsheng, L. Jinsheng, *Physics of Semiconductor*, vol. 133, Publishing House of Electronics Industry, 2003.
- [4] W. Shockley, H.J. Queisser, *J. Appl. Phys.* 32 (1961) 510–519.
- [5] R.L. Bailey, *J. Eng. Power* 94 (1972) 73–77.
- [6] E. Donchev et al., *MRS Energy Sustain.* 1 (2014).
- [7] S. Joshi, G. Moddel, *Appl. Phys. Lett.* 102 (2013) 083901.
- [8] J.A. Hagerty et al., *IEEE Trans. Microw. Theory Tech.* 52 (2004) 1014–1024.
- [9] H.M. Barlow, *Nature* 173 (1954) 41–42.
- [10] G. Hüpper, E. Schöll, *Phys. Rev. Lett.* 66 (1991) 2372–2375.
- [11] J. Karch et al., *Phys. Rev. Lett.* 105 (2010) 227402.
- [12] S. Preu et al., *Rev. Sci. Instrum.* 83 (2012) 053101.
- [13] M. Kimmitt et al., *Int. J. Infrared Millimeter Waves* 13 (1992) 1065–1073.
- [14] G.M. Mikheev et al., *Nano Lett.* 12 (2012) 77–83.
- [15] J. Maysonnave et al., *Nano Lett.* 14 (2014) 5797–5802.
- [16] S. Stachel et al., *Phys. Rev. B* 89 (2014).
- [17] M. Choi et al., *Nature* 470 (2011) 369–373.
- [18] M.A. Seo et al., *Nat. Photonics* 3 (2009) 152–156.
- [19] G. Vampa et al., *Nat. Phys.* 13 (2017) 659–662.
- [20] K. Fan et al., *Phys. Rev. Lett.* 110 (2013) 217404.

- [21] N.I. Zheludev, Y.S. Kivshar, *Nat. Mater.* 11 (2012) 917–924.
- [22] J. Lee et al., *Nature* 511 (2014) 65–69.
- [23] M.W. Klein et al., *Science* 313 (2006) 502–504.
- [24] X. Yin et al., *Science* 339 (2013) 1405–1407.
- [25] N. Kumar et al., *Opt. Express* 20 (2012) 11277–11287.
- [26] N. Liu, H. Giessen, *Angew. Chem. Int. Ed. Engl.* 49 (2010) 9838–9852.
- [27] Y. Wen, J. Zhou, *Phys. Rev. Lett.* 118 (2017) 167401.
- [28] H. Hirori et al., *Appl. Phys. Lett.* 98 (2011) 091106.
- [29] M. Shalaby, C.P. Hauri, *Nat. Commun.* 6 (2015) 5976.
- [30] C. Vicario et al., *Phys. Rev. Lett.* 118 (2017).
- [31] C. Lange et al., *Phys. Rev. Lett.* 113 (2014).
- [32] K.E. Strecker et al., *Nature* 417 (2002) 150–153.
- [33] M.I. Dyakonov, A. Khaetskii, *Spin Physics in Semiconductors*, vol. 1, Springer, 2008.
- [34] Z.-G. Dong et al., *Phys. Rev. B* 87 (2013).
- [35] C. Ciraci et al., *Phys. Rev. B* 85 (2012) 201403.
- [36] G.A. Wurtz et al., *Nat. Nanotechnol.* 6 (2011) 107–111.
- [37] M. Dressel, M. Scheffler, *Ann. Phys.* 15 (2006) 535–544.
- [38] C.K. Sun et al., *Phys. Rev. B* 48 (1993) 12365–12368.
- [39] N. Del Fatti et al., *Phys. Rev. Lett.* 81 (1998) 922.
- [40] P.G. Huggard et al., *J. Appl. Phys.* 87 (2000) 2382–2385.
- [41] C. Kern, M. Kadic, M. Wegener, *Phys. Rev. Lett.* 118 (2017) 016601.
- [42] K. Storm et al., *Nat. Nanotechnol.* 7 (2012) 718–722.
- [43] J. Sun, J. Kosel, *Finite-element Modelling and Analysis of Hall Effect and Extraordinary Magnetoresistance Effect*, INTECH Open Access Publisher, 2012.